Positronium collisions with polar molecules

R. S. Wilde, M. K. Selvage

Department of Natural Sciences, Oregon Institute of Technology, Klamath Falls, Oregon 97601, USA

I. I. Fabrikant

Department of Physics and Astronomy, University of Nebraska, Lincoln, Nebraska 68588-0299, USA

(Dated: September 2, 2022)

Abstract

We calculate elastic and positronium (Ps) break-up cross sections for collisions of Ps with the polar molecules CO, HCl and LiF in the fixed-nuclei approximation. We incorporate electron exchange and correlation for these processes by using the free-electron-gas model developed earlier for Ps scattering by rare-gas atoms, N_2, O_2 and CO_2 molecules. The present target molecules provide a range of dipole moments from the weakly polar CO to the strongly polar LiF. We find that Ps scattering is similar to electron scattering when the cross sections are plotted as a function of projectile velocity for the targets with smaller dipole moments (CO, HCl). However, we do not see such a similarity for LiF which has a large dipole moment. Below the Ps break-up threshold we observe resonance structures similar to those obtained earlier for the other molecular targets that we have studied.

I. INTRODUCTION

Not long ago the similarity between electron and positronium (Ps) scattering cross sections when plotted as a function of projectile velocity was demonstrated experimentally [1]. This similarity exists over a wide velocity range for velocities (energies) above the Ps ionization (break-up) threshold which occurs at a velocity of 0.5 a.u. (or Ps kinetic energy 6.8 eV). Near the threshold, resonances in Ps-N_2 [2] and Ps-CO_2 [3] scattering have been observed experimentally. These resonances are similar to those observed in electron scattering by these targets (see [4–6] and references therein). Similar resonances near the ionization threshold have been seen in our previous theoretical calculations which employ a Free Electron Gas (FEG) model to determine the scattering potentials. [7, 8].

A proof of the similarity between electron and Ps cross sections for the same projectile velocity was given in Ref. [9]. It is based on the impulse approximation and is valid for high enough projectile energies, at least above the Ps break-up threshold. The physical reason for this result is the dominance of the electron scattering amplitude, as compared to the positron scattering amplitude, due to electron exchange with the target electrons [10]. The impulse approximation equations also show that the dominant scattering in Ps collisions is due to quasifree electrons having momentum $\mathbf{q} = -\Delta\mathbf{p}/2$, where $\Delta\mathbf{p}$ is the Ps momentum transfer, resulting in equal cross sections for equal velocities. This similarity extends to the resonant scattering, if the resonance position is above the Ps break-up threshold. We should emphasize that this result is valid only at high enough energies. At low energies the long-range interaction between the target and the projectile dominates, and it is determined by two different potentials: the dipole or polarization potential for electron scattering and the van der Waals potential for Ps scattering. This difference, for example, results in the absence of the Ramsauer-Townsend minimum in Ps scattering by heavy rare-gas atoms [11]

Recently we performed FEG calculations for the O_2 and CO_2 molecules which also exhibited resonant features near or below the Ps ionization threshold [8]. At higher Ps velocities good agreement between the total electron and Ps scattering cross sections as a function of projectile velocity was found.

As was emphasized above, it shouldn't necessarily be expected that the similarity between electron and Ps scattering extends to low velocities. In addition to the aforementioned long-range effects, there are also considerations based on angular momentum conservation. In

contrast to electron-molecule scattering, in the case of Ps-molecule scattering the electron in Ps does not possess a certain projection of angular momentum on the internuclear axis, therefore the symmetry of the resonance is different in the two cases. In particular in the case of Ps$-N_2$ scattering, instead of one resonance of Π_g symmetry, we obtain three resonances of Σ_u, Π_u and Δ_g symmetries [7]. For electron scattering by a polar molecule the long-range interaction is dominated by the dipole potential which decays inversely with the square of the electron-molecule distance. This can lead to large cross sections for slow electrons and, in fact the total cross section in this case is formally divergent in the fixed-nuclei approximation [12, 13]. For Ps scattering by a polar molecule the long-range interaction is due to the van der Waals potential which decays as the sixth power of the distance. The van der Waals coefficient in this case is due to the interaction of the dipole moment and the neutral Ps (Debye interaction) as well as the charge distribution of the molecule and Ps (London interaction), but due to the rapid decay of the van der Waals potential it should be expected that the dipole moment has much less effect on the low velocity (energy) behavior for Ps scattering than it does for electron scattering. Therefore it is of a certain interest to extend comparison of electron and Ps scattering to polar targets. The UCL group performed this comparison for the water molecule [14, 15] by measuring electron and Ps cross sections. They found similar cross sections for the projectile velocity above 1 a.u. For lower velocities the Ps cross section is substantially lower as should be expected. The water molecule, being nonlinear, presents a challenge for Ps scattering calculations, therefore in the present paper we start these investigations for linear diatomic targets.

Another challenging aspect of the theoretical treatment of the Ps-atom and Ps-molecule interaction is an accurate inclusion of electron exchange and electron and positron correlation. The exact treatment of these effects based on the close-coupling method [16–18] becomes very computationally expensive as the size of the target grows, and therefore so far this type of calculation has been carried out only for simple atomic systems like hydrogen and light rare-gas atoms. A few approximate methods for inclusion of exchange and correlation have been developed which include the pseudopotential method [10, 19], methods based on many-body theory [20], and methods based on confined basis sets [21–24].

Our FEG model for Ps-atom or Ps-molecule scattering has been developed in ref. [25]. The FEG potentials were used to calculate elastic scattering cross sections for Ps-N_2 [7, 26] and Ps-rare-gas-atom collisions [11] as well as for Ps-O_2 and Ps-CO_2 [8]. The calculations

were successful in the description of the relevant experiments, particularly in explanation of the resonance structure in the cross sections for Ps-N_2 scattering.

The molecules studied in our previous work all have an inversion symmetry which allows the scattering matrices to be described as gerade or ungerade. In the present paper we extend our calculations to polar molecules. The present targets were selected for their range of dipole moments starting with the slightly polar CO, then going to the moderately polar HCl, and finishing with the highly polar LiF. In order to obtain total Ps scattering cross sections we add the elastic and Ps ionization cross sections. To determine the ionization cross sections we use the binary-encounter model [7, 23] which relies on the elastic scattering of electrons and positrons with the target molecules.

In section II we discuss important aspects of our electron and positron scattering calculations including Born closure and the FEG correlation potential for positron scattering. In section III we present our Ps ionization cross sections using the binary-encounter model. In section IV we describe the Ps-molecule scattering potentials used in the present calculations to obtain elastic cross sections and in section V we present our elastic and total Ps scattering cross sections. Section VI is a brief conclusion. As has become customary since the discovery of the similarity between electron and Ps scattering [1], we plot most cross sections as functions of the projectile velocity. Atomic units are used throughout unless stated otherwise.

II. ELECTRON AND POSITRON SCATTERING

In the present paper we compare integrated cross sections for electron and Ps scattering assuming that the main contribution to the total cross section for electrons is due to elastic scattering, and for Ps due to elastic scattering and Ps ionization (break-up). Since we use the fixed-nuclei approximation (with the exception of the Born closure, see below), our "elastic" cross section include implicitly rotationally inelastic transitions. For calculation of the Ps ionization cross sections we need electron and positron elastic cross sections. To estimate the quality of our results, we have calculated elastic electron and positron cross sections for the selected targets. Another reason for performing electron scattering calculations is to compare electron and Ps cross sections when exchange and correlation effects treated in the same way (FEG model in our case) are included for both projectiles. In this section we

describe some important aspects of these calculations.

The elastic scattering cross sections are obtained from the scattering matrices $T^m_{ll'}$ in the fixed-nuclei approximation. Here lm are electron angular momentum and its conserved projection on the internuclear axis. We compute the scattering potentials from the charge density of the target molecule at the equilibrium internuclear separation. For electron scattering we use the Hara Free Electron Gas Exchange (HFEGE) model [27] and the FEG correlation potential of O'Connnell and Lane [28]. For positron scattering we use a modifed FEG correlation potential described below in subsection II B. The charge densities for all molecules studied here were calculated using the 6-31G* basis set in the PySCF quantum chemistry package [29–31]. The values of the dipole moment were obtained from the asymptotic behavior of the potentials, and polarizabilities of CO and HCl from the NIST data [32]. By analyzing the computed values of polarizabilities calculated in Ref. [33], we have chosen for the averaged polarizability of LiF 10.9 a.u.. A summary of the literature data and the present data on the dipole moments D and polarizabilities α is presented in Table I.

TABLE I. Dipole moments D and polarizabilities α of the target molecules, comparison with the NIST data [32] (experiment and theory) for CO and HCl. Theoretical values for LiF are from [33] All quantities are listed in a.u.

target		present	exp	theory[a]
CO	D	0.058	0.044	0.052-0.068
HCl		0.46	0.43	0.47-0.57
LiF		2.52	2.49	2.34-2.60
CO	α	13.19	13.19	
HCl		17.0	17.0	
LiF		10.9		10.45-11.10

[a] different versions of coupled-cluster calculations and MP perturbation theory.

We solve the coupled equations with the appropriate static, exchange and correlation potentials using the integral equation method of [34] to obtain elastic e^- and e^+ (as well as Ps) scattering matrices and cross sections. The FEG potentials used for Ps scattering are described in section IV.

A. Closure formulae and electron scattering cross sections

Several different versions of the closure formulae for electron-polar-molecule scattering were discussed in the review [13]. Here we give a summary of the approach used in the present paper.

The total elastic cross section in the fixed-nuclei approximation ($T^m_{ll'}$ is the fixed nuclei T-matrix)

$$\sigma = (2-\delta_{m0})\frac{\pi}{k^2}\sum_{ll'm\geq 0}|T^m_{ll'}|^2$$

is diverging in m as a harmonic series, therefore to get a finite result we use closure with account of rotations

$$\sigma_{jj'} = {}^B\sigma_{jj'} + \sum_m(\sigma^{(m)} - {}^B\sigma^{(m)}) \tag{1}$$

where ${}^B\sigma_{jj'}$ is the cross section for rotational transition $j \to j'$ in the Born approximation

$${}^B\sigma_{jj'} = \frac{8\pi D^2}{3k_0^2}\frac{j_>}{2j+1}\ln\frac{k_0+k}{|k_0-k|}$$

and ${}^B\sigma^{(m)}$ is the partial fixed-nuclei cross section in the Born approximation including $|m|$ and $-|m|$ contributions

$${}^B\sigma^{(m)} = \frac{8\pi D^2}{k^2}[2m^2\psi'(m) - 2m - 1] \quad \text{for} \quad m \neq 0$$

where ψ' is the derivative of the digamma function. We note that D is the dipole moment and k_0, k are the initial and final electron momenta, respectively. For $m = 0$

$${}^B\sigma^{(0)} = \frac{4\pi D^2}{k^2}.$$

Eq. (1) will be called the m closure. The m closure might not be sufficient for convergence since the partial cross section

$$\sigma^{(m)} = (2-\delta_{m0})\frac{\pi}{k^2}\sum_{ll'}|T^m_{ll'}|^2,$$

is slowly convergent with l. To speed up this convergence, we employ the fixed-nuclei T matrix in the Born approximation

$${}^BT^m_{ll'} = 2iD[q^m_l\delta_{l'l-1} + q^m_{l+1}\delta_{l'l+1}] \tag{2}$$

where

$$q^m_l = \frac{1}{l}\left[\frac{(l+m)(l-m)}{(2l-1)(2l+1)}\right]^{1/2}.$$

Using the symmetry of the T matrix, we obtain

$$\sigma^{(m)} = \frac{\pi}{k^2} \sum_{l=m}^{\infty} \sum_{l' \geq l}^{\infty} (2 - \delta_{m0})(2 - \delta_{ll'}) |T_{ll'}^{m}|^2.$$

Similarly, using the Born T matrix, Eq. (2), we have

$${}^{B}\sigma^{(m)} = \frac{8\pi D^2}{k^2} (2 - \delta_{m0}) \sum_{l=m}^{\infty} (q_{l+1}^{m})^2.$$

Therefore the second (l) closure equation becomes

$$\sigma^{(m)} = {}^{B}\sigma^{(m)} + (2 - \delta_{m0}) \frac{\pi}{k^2} \sum_{l=m}^{\infty} \left[\sum_{l'=l}^{\infty} (2 - \delta_{ll'}) |T_{ll'}^{m}|^2 - 8D^2 (q_{l+1}^{m})^2 \right] \tag{3}$$

In practice the upper limits of summation goes to $l_{\max}$ where $l_{\max}$ is determined from the requirement that convergence of the sum (3) is achieved. For sufficiently large m the Born approximation is valid for any l, therefore

$$\sum_{l'=l}^{l_{\max}} (2 - \delta_{ll'}) |T_{ll'}^{m}|^2 - 8D^2 (q_{l+1}^{m})^2 = 0 \quad \text{(large } m\text{)}.$$

This also can be rewritten as

$$\sigma^{(m)} = \frac{8\pi D^2}{k^2} \sum_{l=m}^{\infty} (q_{l+1}^{m})^2 \quad \text{(large } m\text{)}. \tag{4}$$

Combining Eqs. (1) and (3) we obtain

$$\sigma_{jj'} = {}^{B}\sigma_{jj'} + \frac{\pi}{k^2} \sum_{m=0}^{\infty} (2 - \delta_{m0}) \sum_{l=m}^{\infty} \left[\sum_{l'=l}^{\infty} (2 - \delta_{ll'}) |T_{ll'}^{m}|^2 - 8D^2 (q_{l+1}^{m})^2 \right] \tag{5}$$

or

$$\sigma_{jj'} = {}^{B}\sigma_{jj'} + \sum_{m=0}^{\infty} [\sigma^{(m)} - \frac{8\pi D^2}{k^2} (2 - \delta_{m0}) \sum_{l=m}^{\infty} (q_{l+1}^{m})^2] \tag{6}$$

In Fig. 1 we present the integrated elastic cross section for e^--HCl scattering and compare it with the total integrated cross sections of Hamada and Sueoka [40]. These authors obtained their integrated cross sections by extrapolating measured differential cross sections using the Born formula for the most populated rotational state at $T = 300$ K, $j = 3$. Therefore in our calculations we used Eq. (6) with the same value of j. Agreement is satisfactory, for both shape and absolute values, although the theoretical minimum at low energies is much more pronounced than in the experimental curve. At higher energies inelastic processes, mostly electron impact ionization which are not included in calculations, start to contribute

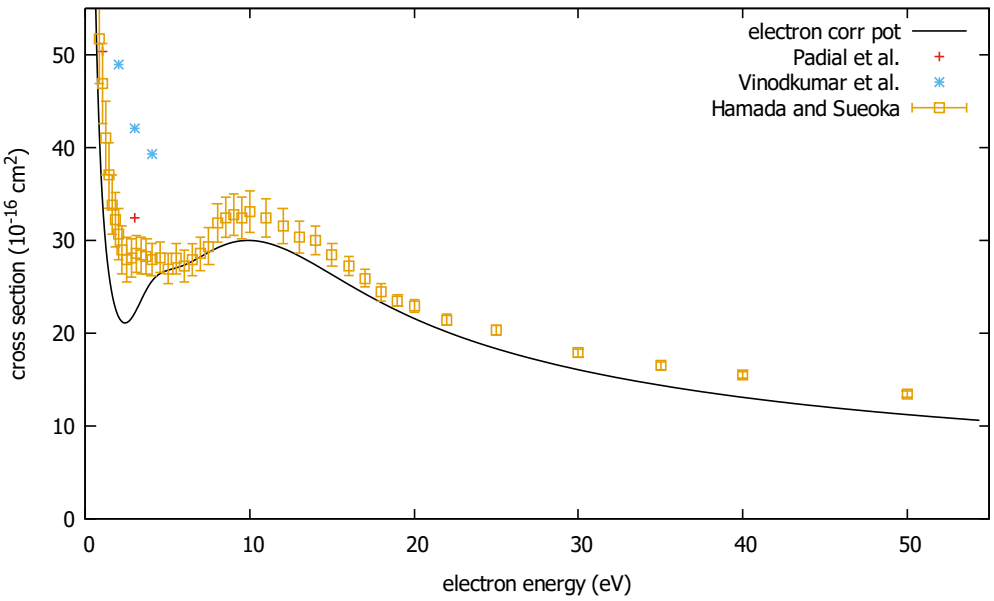

FIG. 1. Electron-HCl elastic cross sections. Solid line, present calculations; error bars, measured *total* cross sections of Hamada and Sueoka [40]. Previous calculations of *elastic* cross section: Padial *et al.* [41] and Vinodkumar *et al.* [42].

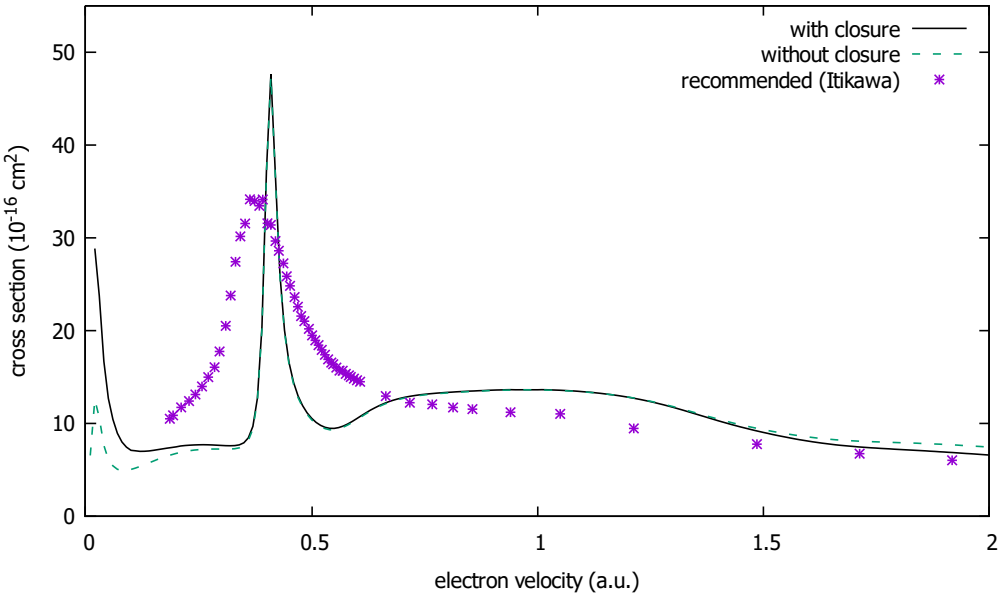

FIG. 2. Elastic e^--CO cross sections without closure (dashed line) and with closure (solid line). Stars, recommended elastic cross sections of Itikawa [38].

to the total cross section. Two previous calculations [41, 42] for a few energy points are also shown. The R-matrix results [42] are too high because of the overestimated value of the dipole moment (0.544 a.u.). As was discussed above, in this and all following figures by "elastic" we mean the cross sections including rotational excitation.

In Fig. 2 we present elastic cross sections for e^--CO scattering with and without closure and compare them with recommended cross sections of Itikawa [38]. The results without closure were obtained with $m_{\max} = 6$, $l_{\max} = 10$. Due to the small dipole moment in this case higher partial waves have a relatively small effect and do not change the cross section much except at very low velocities. Agreement with the recommended cross sections is good, with the pronounced Π resonance appearing at only a slightly higher velocity (energy) compared with the recommended values. Also the computed resonance is much narrower, apparently due to the neglect of inelastic scattering channels, mostly vibrational excitation.

B. Positron correlation potential

The correlation-polarization potential for electron scattering was derived [28] from the correlation energy for a free electron gas. Similar attempts have been made to derive a positron correlation-polarization potential from the many-body theory result of Arponen and Pajanne [43] who obtained the correlation energy of a positron embedded in the electron gas. Boronski and Niemenen [44] worked out an analytical expression describing Arponen and Pajanne's results. Jain [45] and Gianturco *et al.* [46] used this expression to derive the correlation potential for a positron interacting with a molecular system using the expression from density-functional theory [47]

$$V_{\rm corr}(\mathbf{r}) = \left(1 - \frac{1}{3} r_s \frac{d}{dr_s}\right) \epsilon_{\rm corr}(r_s) \tag{7}$$

where r_s is the average-distance parameter related to the electron density $n(\mathbf{r})$ as

$$\frac{4}{3}\pi r_s^3 n(\mathbf{r}) = 1.$$

Using Eq. (7) Jain [45] and Gianturco *et al.* [46] derived the correlation potential, but the final expression in Ref. [46] contains several typos. Note that the review paper of Kimura *et al.*[48] gives the correct expression . The incorrect result [46] was used in [49, 50]. A more recent paper [51] used the correct expression following from Eq. (7).

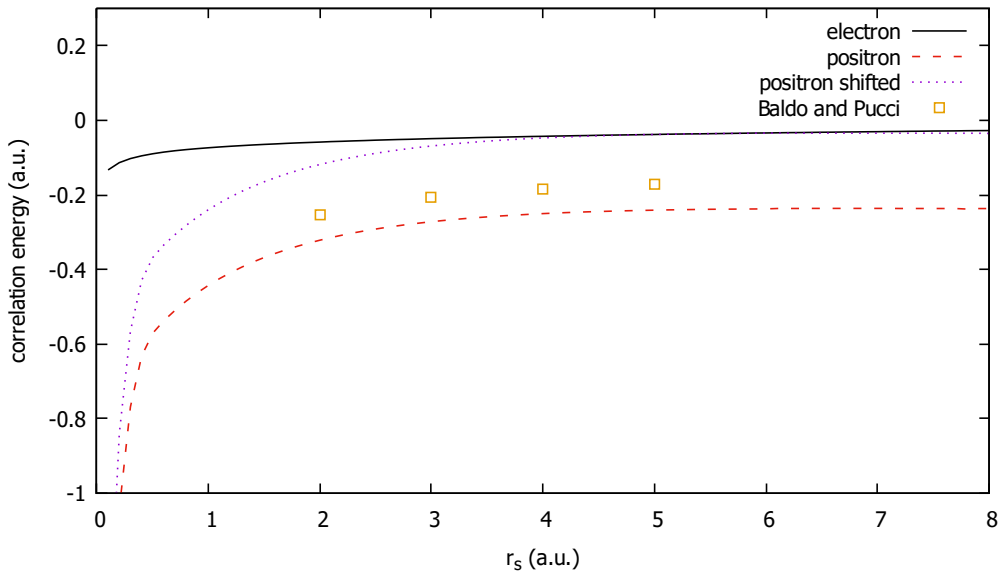

FIG. 3. Correlation energies, comparison of results for positron and electron. The positron results are from Ref. [44] (dashed curve). The same energy shifted upwards by 0.203 a.u. is given by the dotted curve. Squares are results of the linear response theory [56].

With regard to Jain's result [45], we should note that the correlation energy derived in [43, 44] contains dependence on the position vector $\mathbf{r}$ through the parameter r_s, therefore it cannot be identified as the expression for the total correlation energy [47] (independent of $\mathbf{r}$)

$$E_c[n] = \int n(\mathbf{r})\epsilon_c(n(\mathbf{r}))d\mathbf{r}$$

but rather the positron correlation energy $\epsilon_c(n(\mathbf{r}))$. Therefore we believe that a correct use of results [43, 44] should treat the original expression for $\epsilon_{\rm corr}$ as the correlation potential. In fact Jain [45] used both potentials for e^+-Ar scattering and found little difference between the two sets of calculations since the two expressions are rather close to each other.

In Fig. 3 we compare positron and electron [52] correlation energies as functions of the average-distance parameter r_s. The difference between the electron and positron correlation potentials is striking. Whereas the big difference at high densities (low r_s) is justified, at higher r_s, where the perturbation theory becomes valid, polarization contributions for electron and positron should be close to each other. In addition, another calculation of the positron correlation potential by Gianturco *et al.*[53], based on the density functional theory, gives results substantially smaller (in the absolute magnitude). On the other hand, Jain [45]

states that the use of the electron polarization potential for e^+-Ar scattering produces much poorer results than the potential derived from [43, 44].

Returning to the original calculation of Arponen and Pajanne [43], we note that they calculate the *ground*-state correlation energy for a positron in the electron gas. In the low-density limit, that is at $r_s \to \infty$, this corresponds to an energy of Ps^- which is -0.524 Ry$= -0.262$ a.u., and the result of Arponen and Pajanne, -0.522 Ry, virtually agrees with the exact value. This certainly does not satisfy the condition of the positron-molecule scattering problem where in the limit of low electron density the correlation potential should go to 0. It is apparent that the contribution to the correlation energy leading to formation of Ps^- should be excluded from $\epsilon_{\rm corr}$. It is not clear how to do this in a rigorous manner. However, the analysis of Table II of Arponen and Pajanne [43] suggests a way to improve Jain's correlation potential. The table presents the correlation energy in the first-order and second order Tamm-Dancoff approximation (TDA) [54, 55], and also the most accurate results obtained with the coherent-state TDA. The last two include triple correlations, and therefore give the correct Ps^- energy in the low-density limit (high r_s). The first-order TDA in this limit gives the energy of the Ps ground state, -0.5 Ry. The difference between the second-order TDA and the first-order TDA remains almost constant at high densities (about 0.1 Ry), and then decreases to 0.022 Ry at large r_s. This suggests that for the purpose of the description of positron-molecule interaction at low r_s the TDA result should be shifted upward by a constant value of about 0.522 Ry. At larger r_s the potential should be merged into the electron polarization potential. In fact the value of the shift should be somewhat lower than 0.522 Ry since the coherent-state TDA result of Arponen and Pajanne exhibits a shallow maximum at $r_s = 6.7$ a.u. of an unknown origin. Therefore we choose the value of the shift from the requirement that the positron correlation energy joins smoothly with the electron correlation energy at high r_s. The shifted potential with the value of the shift 0.406 Ry=0.203 a.u. is presented in Fig. 3. The linear response function calculations of Baldo and Pucci [56] give the correlation energy which is somewhere between the original results of Arponen and Pajanne and the modified results used in the present calculations.

An alternative treatment of correlation and polarization in positron-atom and positron-molecule collisions involves the polarized orbital method [57]. Several calculations [58–60] using this method have been performed in the past, but we are not aware of any comparisons between the two methods.

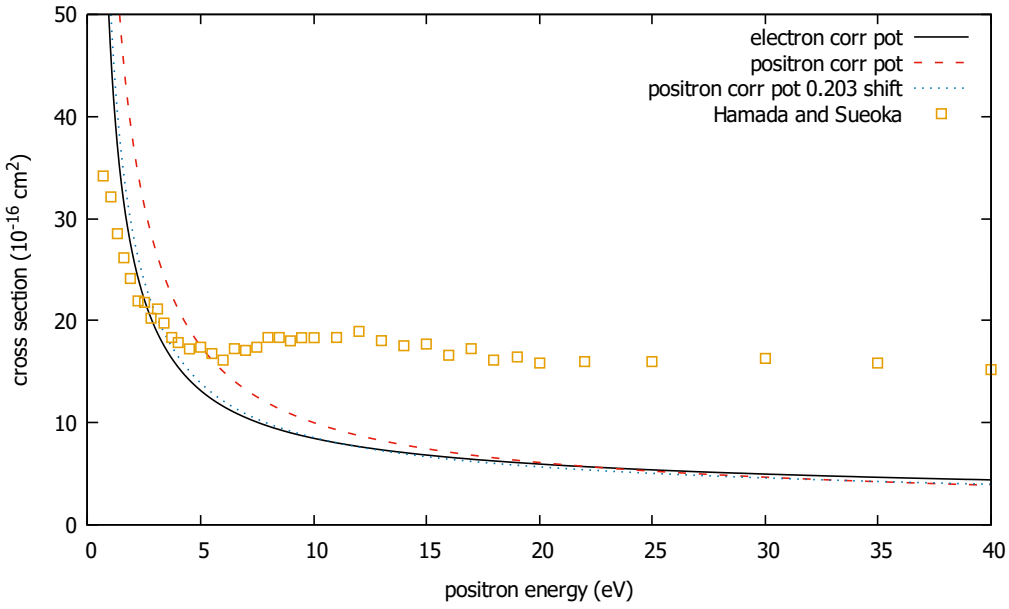

FIG. 4. Positron-HCl elastic cross sections. Solid line, present calculations using the electron correlation potential; dashed line, using the positron correlation potential; dotted line, using the modified positron correlation potential with a shift of 0.203 a.u.; squares, measured *total* cross sections of Hamada and Sueoka [40].

Using the correlation potential constructed as described above, we have calculated elastic cross sections for positron scattering by CO, HCl and LiF.

e^+-HCl elastic scattering cross sections are presented in Fig. 4 where we give comparison with Hamada and Sueoka [40]. Agreement is not as good as for electrons, mainly because our cross section does not include the Ps formation channel which is opening at $E = 5.94$ eV. At higher energies other inelastic channels are contributing as well. The excitation and ionization channels can be taken into account by adding an absorption potential [61]. Although the derivation of the absorption potential [61] is based on the binary-encounter model, there were attempts [58, 62, 63] to modify this model for inclusion of the Ps formation channel. The approach is empirical and its detailed discussion is beyond the scope of the present work.

e^+-CO elastic scattering cross sections are presented in Fig. 5 where we see results similar to the e^+-HCl case. We compare our results with the measurements of the total cross section by Zecca *et al.* [64]. At low velocities the results with the shifted positron correlation potential agree better with the measurements than those with the nonmodified

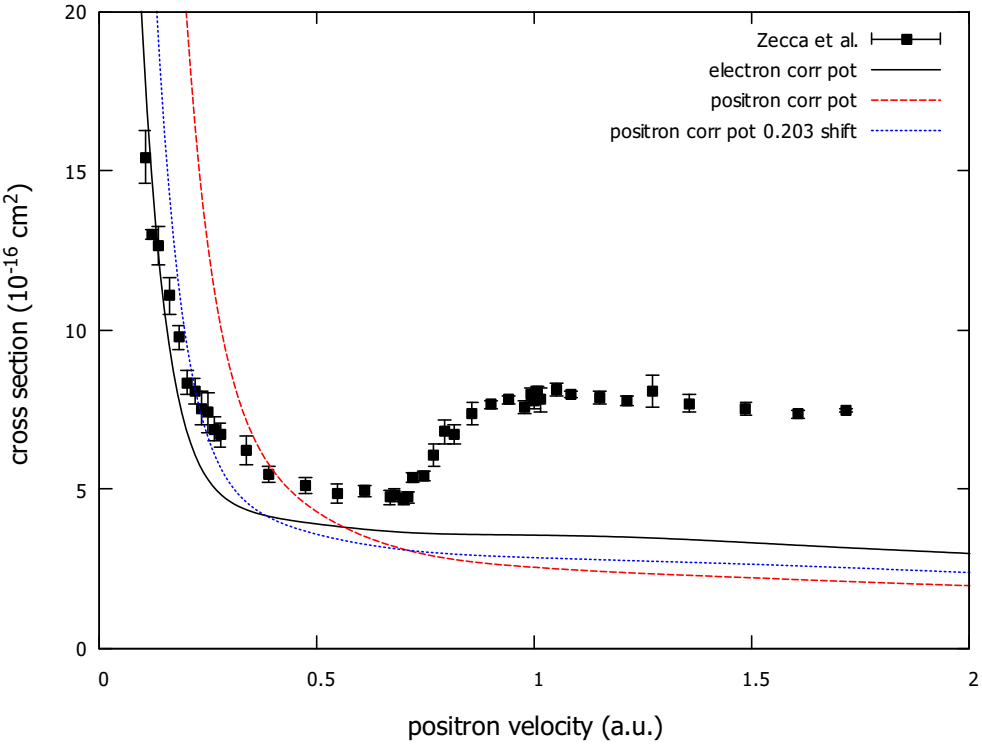

FIG. 5. Positron-CO elastic cross sections. Solid line, present calculations using the electron correlation potential; dashed line, using the positron correlation potential; dotted line, using the modified positron correlation potential with a shift of 0.203 a.u.; squares, measured *total* cross sections of Zecca *et al.* [64].

positron correlation potential. Our results at intermediate velocities (around 0.5 a.u.) are slightly lower than the measured values, however there is some disagreement between various measurements below the Ps formation threshold, see [64] and references therein. For example cross sections measured by Sueoka and Hamada [65] are substantially lower than those in [64]. In calculations of the Ps ionization cross section using the binary encounter model we have used the modified positron correlation potential results.

Lastly, for this section, we present our elastic e^--LiF and e^+-LiF cross sections compared with the electron scattering measurements of Vušković *et al.* [66] in Fig. 6. Cross sections, both with and without closure, for e^+-LiF scattering are shown. It is apparent that higher partial waves are very important in this case due to the large dipole moment of LiF. We find good agreement between our e^--LiF cross sections and the measured values which were obtained by extrapolation of the differential cross sections using the Born formula. Due to

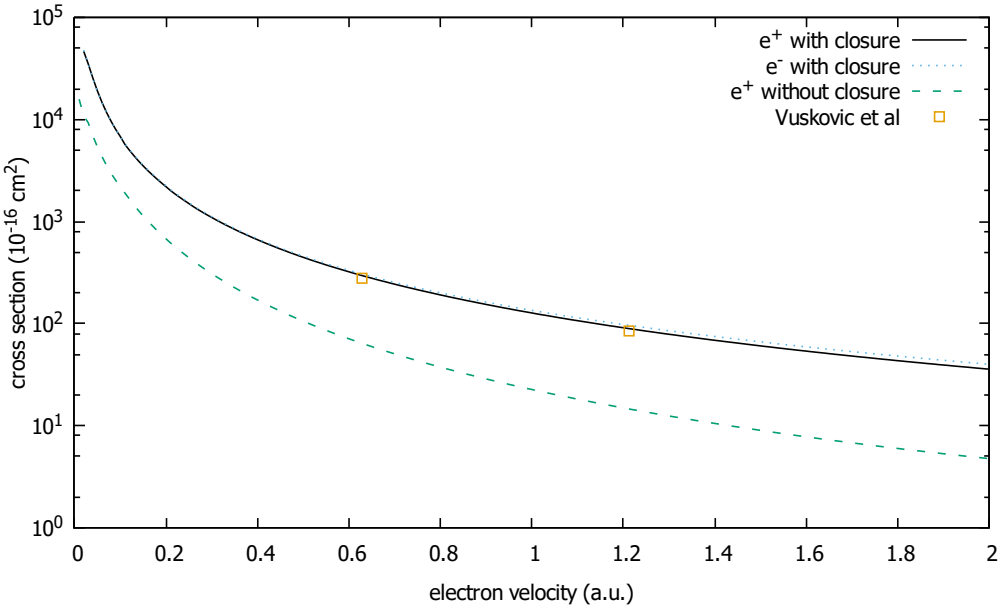

FIG. 6. Elastic e^--LiF and e^+-LiF cross sections. Solid line, positron scattering with closure; dotted line: electron scattering with closure; dashed line electron scattering without closure. Squares are measured *elastic* cross sections of Vuskovic *et al.* [66].

the effect of the large dipole moment the electron and positron scattering cross sections are almost identical.

III. PS IONIZATION

Apart from elastic scattering, the largest contribution to the total cross section for positronium collisions is expected to be Ps ionization (fragmentation) or break-up. In the present paper we employ the binary encounter approximation to calculate cross sections for Ps ionization [35, 36]. We have previously applied this approximation to calculate Ps ionization cross sections in collision with rare gas atoms Ar, Kr and Xe [19] which were in good agreement with previous calculations using the impulse approximation [37]. The binary encounter approximation for Ps ionization was extended to non-spherical interactions and applied to Ps scattering by N_2, O_2 and CO_2 in [7, 8].

Briefly, the binary encounter approximation is based on the assumption that the electron and positron in Ps interact independently with the target molecule and the ionization cross

section due to either electron or positron collision may be written as

$$\sigma_{ion}^{\pm} = \frac{1}{v_B}\langle|\mathbf{v}-\mathbf{v}_B|\int_{\Delta E>I} d\sigma^{\pm}\rangle. \tag{8}$$

where $\mathbf{v}_B$ is the relative collision velocity, $\mathbf{v}$ is the electron (positron) velocity relative to the Ps center-of-mass, $d\sigma^{\pm}$ is the differential cross section for $e^+ - B$ or $e^- - B$ elastic scattering, and the integration is restricted by the angles which result in the energy transfer to electron (positron) ΔE greater than the Ps ionization potential $I = 6.8$ eV.

The ionization amplitude in the binary encounter approximation depends on the elastic differential cross section through the body frame T-matrix elements, $T_{ll'}^{m}$, in the fixed nuclei approximation for electron and positron scattering by the target calculated as described in the previous section. In the present calculations we have used $l_{\max} = 10$ and $m_{\max} = 6$. Unlike the elastic e^- and e^+ scattering cross sections the Ps ionization cross sections are well converged by $m = 6$ since small scattering angles don't contribute as significantly to ionization.

In Fig. 7 we show our Ps ionization cross sections for all three presently studied targets. The cross section is overall largest for LiF, somewhat smaller for HCl and smallest for CO which aligns generally with the size of the elastic e^- and e^+ cross sections for the same target. In particular, due to the similarity between e^--LiF and e^+-LiF cross sections the contribution of each (electron and positron) is about the same, whereas for the other target molecules the positron contribution is smaller.

IV. PS SCATTERING POTENTIALS

For elastic scattering of Ps by the presently considered molecules we determine the scattering potentials in the same way as was done for Ps-N_2 scattering [7] as well as for Ps-O_2 and Ps-CO_2 [8]. In ref. [25] we have derived expressions for the exchange and correlation energies as functions of the Fermi energy. In order to introduce the dependence of these energies on the projectile position relative to the target we determine the Fermi energy in terms of the charge density of the ground state of the molecule. The Ps-molecule scattering potentials obtained in this way are then expanded in Legendre polynomials. The charge density for all molecules studied here were calculated as described in section II.

The correlation potential for Ps scattering at large distances is matched smoothly with

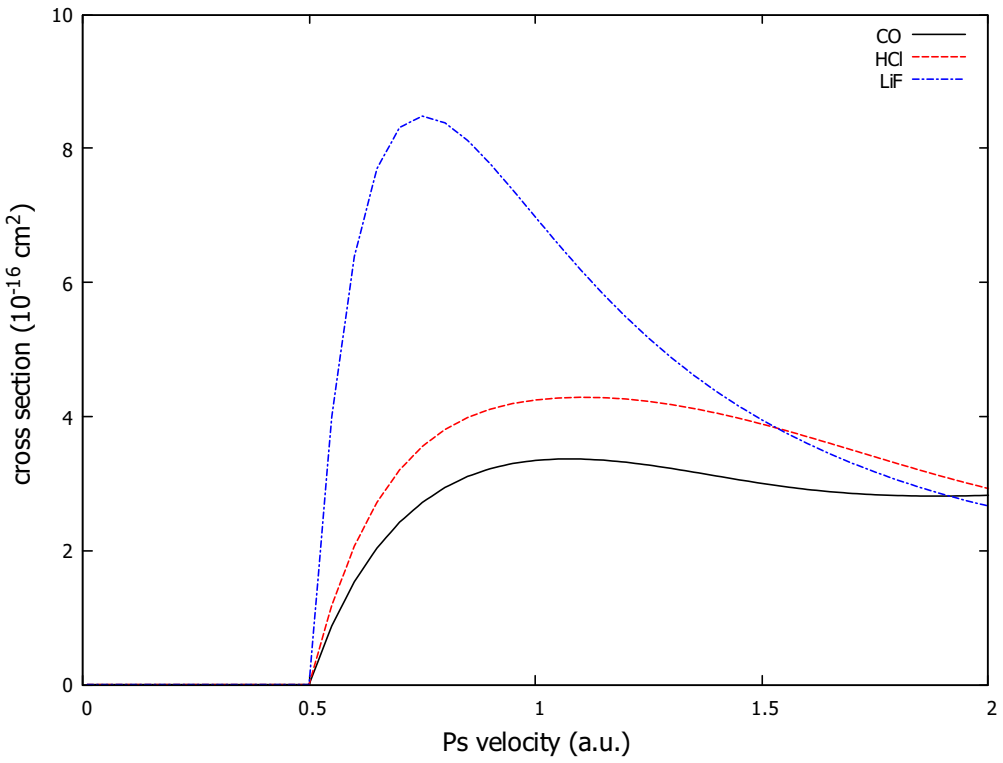

FIG. 7. Binary-encounter Ps ionization cross sections for collisions with CO (solid line), HCl (red dashed line) and LiF (blue dash-dot line) as functions of Ps velocity.

the van der Waals potential with a cut-off of the form

$$V_W(\mathbf{R}) = -\frac{C_W}{(R^2 + R_c^2)^3} \tag{9}$$

where R is the position of the center of Ps relative to the center of mass of the molecule and R_c is a cutoff radius. The van der Waals coefficient C_W is determined by two effects in the present case. The first is the London interaction which arises due to the interaction between induced dipole moments of the neutral Ps and the neutral molecule. The coefficient for this term is calculated by using the London formula

$$C_0 = \frac{3I_1 I_2 \alpha_1 \alpha_2}{2(I_1 + I_2)} \tag{10}$$

where I_1 and I_2 are the ionization potentials of the target molecule and Ps and α_1 and α_2 the spherical polarizabilities.

The second contribution is due to the Debye interaction which arises due to the interaction between the permanent dipole moment of the polar molecule and induced dipole moment of

Ps

$$C_1 = 2D^2\alpha_{Ps} \tag{11}$$

where D is the permanent dipole moment of the polar molecule and α_{Ps}=36 a.u. is the polarizability of Ps. Both of these interactions vary as $1/R^6$. The London and Debye contributions are summed to give the total van der Waals coefficient so that $C_W = C_0 + C_1$.

For CO we use the polarizability α_0=13.19 a.u. and ionization potential of $I = 0.515$ a.u. giving $C_0 = 119.87$ a.u. The dipole moment used for CO is 0.058 a.u. giving C_1= 0.24 a.u. so that C_W= 120.11 a.u. In this case the small dipole moment of CO has a very small effect on the van der Waals coefficient. The cut-off radius R_c was chosen from the requirement that the FEG potential joins smoothly with the potential of Eq. (8). This resulted in $R_c = 0.98$ a.u. and the switching radius $R = 4.06$ a.u.

For HCl we use a polarizability of $\alpha_0 = 17.0$ a.u. and ionization potential of $I = 0.49$ a.u. giving $C_0 = 151.97$ a.u. The dipole moment for HCl is still relatively small (0.46 a.u.) which leads to the still relatively small $C_1 = 15.24$ a.u. so that $C_W = 167.21$ a.u. and, as for CO, the van der Waals interaction is dominated by the London interaction. Again in order for the correlation potential to match smoothly to the asymptotic form we have chosen a cutoff radius of $R_c = 1.01$ a.u. and switch to the asymptotic form at $R = 4.09$ a.u.

For LiF we use a polarizability of $\alpha_0 = 10.6$ a.u. and ionization potential of $I = 0.472$ a.u. giving $C_0 = 93.55$ a.u.. LiF has a much stronger dipole moment of 2.52 a.u. giving $C_1 = 457.22$ a.u. and $C_W = 550.78$ a.u. so that in this case the van der Waals coefficient is dominated by the Debye interaction. In this case we have chosen a cutoff radius of $R_c = 1.05$ a.u. and for the spherical component $\lambda = 0$ switched from the correlation potential to the asymptotic form at $R = 3.06$ a.u.

In Fig. 8 a) we show the first two components (λ=0,1) of the Legendre expansion for the total Ps-CO potential (exchange plus correlation) for a Ps velocity of 0.01 a.u. We note again that in the present case for heteronuclear polar molecules there is no inversion symmetry and the λ=1 component is non-zero unlike the situation for a homonuclear target molecule. In Fig. 8 b) we show the (λ=0,1) components for the total Ps-LiF potential. The $\lambda = 1$ component is more attractive in the case of LiF, but overall the potentials are quite similar for both molecules despite the large difference in dipole moments.

In Fig. 9 we show the first two components (λ=0,1) of the Legendre expansion for the total Ps-HCl potential for a Ps velocity of 0.01 a.u. In this case the $\lambda = 0$ component is more

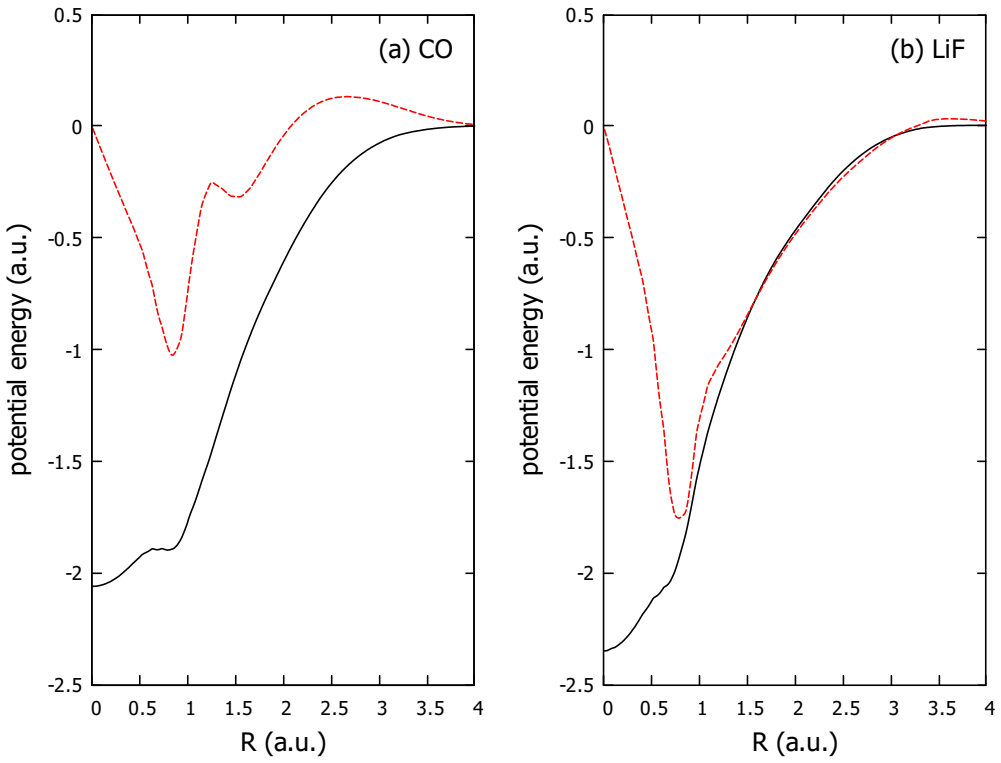

FIG. 8. First two components of the total (exchange plus correlation) Ps-molecule scattering potential for a) Ps-CO and b) Ps-LiF at a Ps velocity of 0.01 a.u. Solid line: $\lambda = 0$, Red dashed line: $\lambda = 1$.

dominant due to center-of-mass being located very close to the Cl atom and the potential is generally stronger at small values of R than that for CO and LiF.

V. ELASTIC AND TOTAL PS SCATTERING CROSS SECTIONS

In Fig. 10 we present the calculated elastic and total (elastic plus ionization) cross sections for Ps-CO scattering along with the recommended total e^--CO cross sections of [38]. We compare Ps cross sections with the total electron cross sections because the fact of similarity between electron and Ps scattering was established for the total cross section. At higher velocities the total Ps scattering cross section (elastic plus ionization) is similar to the total electron scattering cross section. Near the Ps ionization threshold (v=0.5 a.u.) we see resonance structures similar to those seen before for Ps-N_2, O_2 and CO_2 scattering [7, 8].

In Fig.11 we present the calculated elastic and total (elastic plus ionization) cross sections

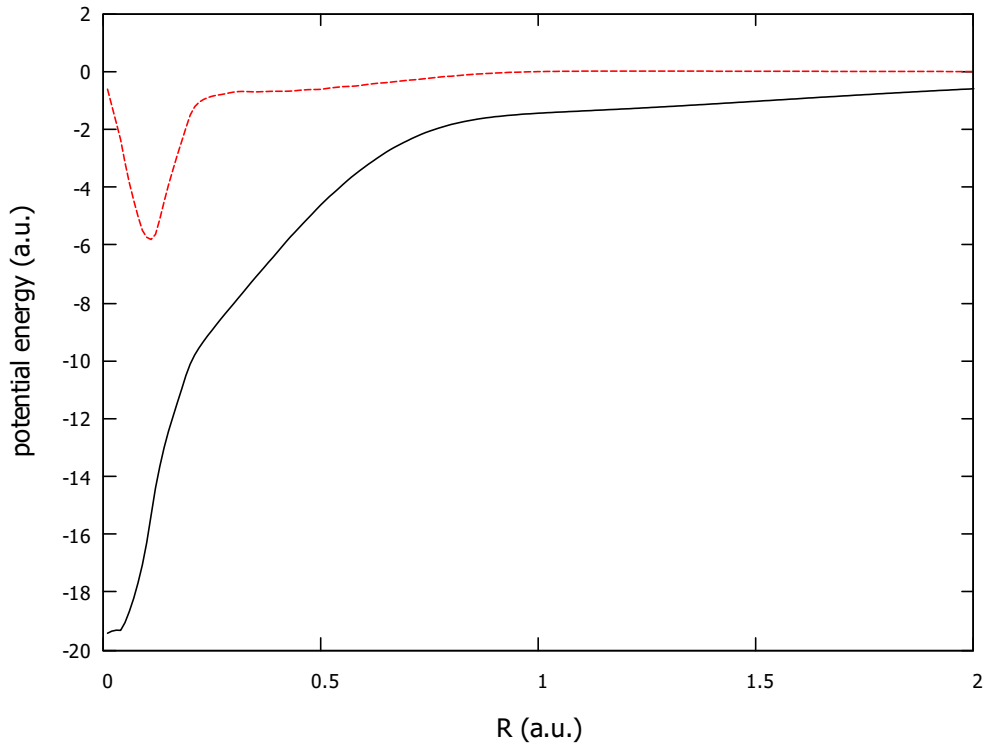

FIG. 9. First two components of the total (exchange plus correlation) Ps-molecule scattering potential for Ps-HCl at a Ps velocity of 0.01 a.u. Solid line: $\lambda = 0$, Red dashed line: $\lambda = 1$.

for Ps-HCl scattering along with the total e^--HCl cross sections of Hamada and Sueoka [40]. Again we see a strong similarity between the total Ps and e^- cross sections. We note though that the similarity at velocities below the ionization threshold ($v = 0.5$ a.u.) is not due to the dipole moment which causes the e^- cross section to rise dramatically. In the Ps-HCl cross section the resonances appear at a lower Ps velocity than for CO and other non-polar molecules due to the more attractive Ps-HCl potential. The resonances cause sharp peaks in the cross section at very low Ps velocities.

Similarly to electron and positron scattering the projection of the Ps center of mass angular momentum on the internuclear axis m is conserved and we can define partial cross sections in terms of this quantum number. In Fig. 12 we present Ps-CO and Ps-HCl partial cross sections for $m = 0, 1, 2$. In both cases we see that the resonance structures are mostly due to the $m = 1$ (Π symmetry) and $m = 2$ (Δ symmetry) which is similar to our previous results for Ps-N_2,O_2 and CO_2 scattering [7, 8]. However, For Ps-HCl, as mentioned before these resonances appear at a lower velocity and the magnitude of the $m = 0$ (Σ symmetry)

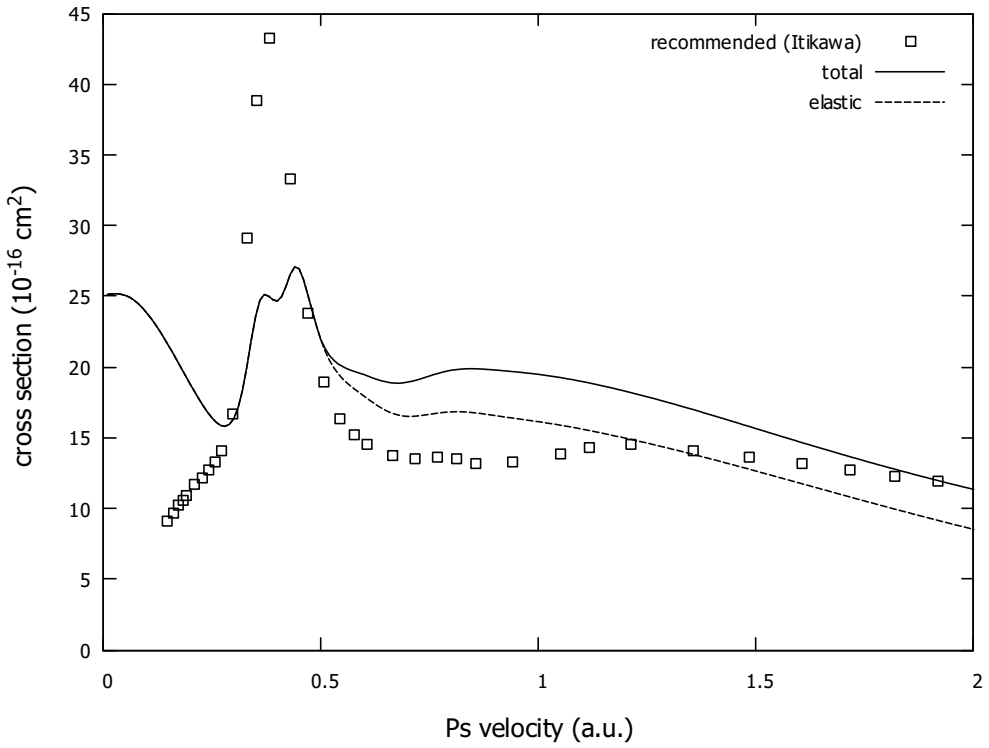

FIG. 10. Elastic Ps-CO (dashed line)and total Ps-CO (solid line) cross-sections compared with recommended total e^--CO cross sections (crosses) of [38] as a function of projectile velocity.

partial cross section is reduced.

In Fig.13 we present the calculated elastic and total (elastic plus ionization) cross sections for Ps-LiF scattering, and in Fig. 14 we present our Ps-LiF partial cross sections for $m = 0, 1, 2$. In this case we again see resonance structures in the Π and Δ symmetries although they are broader than for CO and HCl. While the Σ partial cross section is small at low velocities, overall the total Ps cross section is similar to that for Ps-CO. The difference at low velocities is due to the substantially larger van der Waals coefficient C_W in the case of Ps-LiF which arises due to the much larger dipole moment of LiF and therefore stronger Ps-LiF Debye interaction. In order to see this effect we have also plotted elastic Ps-LiF cross sections in Fig. 13 for which we have neglected the Debye interaction and used $C_W = C_0 = 93.55$ which is due only to the London interaction. We see that when the Debye interaction is neglected the cross section is reduced slightly at higher velocities, but becomes larger and more similar to that for Ps-CO near zero velocity. Thus the large dipole moment of LiF only has a relatively small effect on the elastic Ps-LiF cross section.

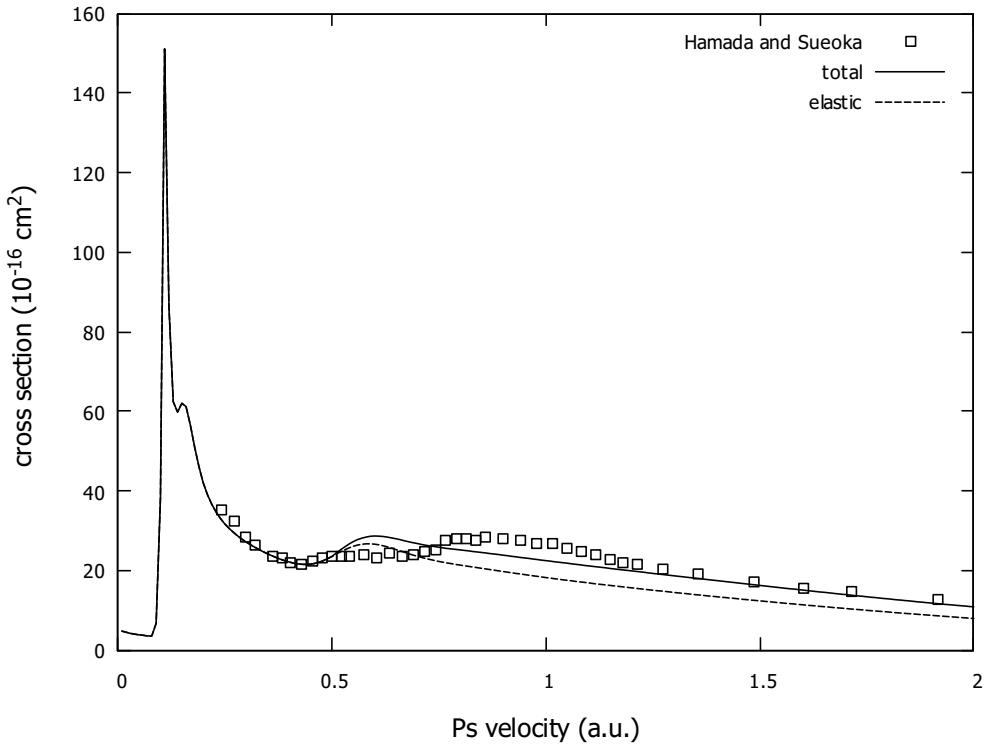

FIG. 11. Elastic Ps-HCl (dashed line)and total Ps-HCl (solid line)cross-sections. Squares are experimental e^--HCl total cross sections of Hamada and Sueoka [40].

Lastly, and perhaps most importantly, we note that the total Ps-LiF scattering cross section is much smaller than the the measured and calculated e^--LiF cross sections plotted in Fig. 6. The difference is about an order of magnitude at the same projectile velocities. While these cross sections include only elastic and rotationally inelastic channels, we expect them to be close to the total e^--LiF scattering cross section. Since LiF has a large dipole moment, the strong dipole interaction has a much bigger effect for e^--LiF scattering than it does for Ps-LiF scattering, and we do not see a similarity between the total cross sections in this case.

VI. CONCLUSION

We have calculated both elastic and Ps ionization cross sections for Ps scattering by several polar molecules using FEG and binary-encounter models. In order to obtain ionization cross sections we have also performed calculations using FEG gas models for electron and positron scattering by these target molecules. For electron and positron scattering we have

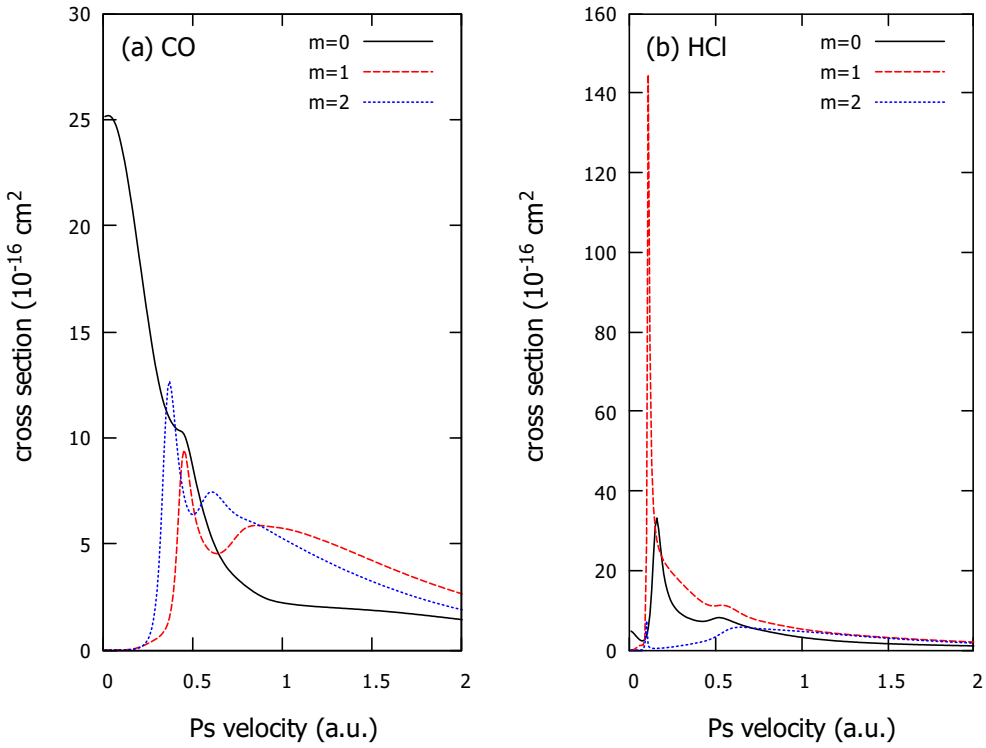

FIG. 12. Partial a) Ps-CO and b) Ps-HCl elastic scattering cross sections. Solid line: $m = 0$, red ashed line: $m = 1$ and blue dotted line: $m = 2$, where m is the quantum number describing the projection of the Ps center of mass angular momentum on the internuclear axis.

studied the effect of higher partial waves and have found it to be important to obtain cross sections that agree with experiment for polar molecules.

As for the case of electron and positron scattering by non-polar molecules [7, 8] the relatively simple FEG model gives fairly good agreement with experimental elastic cross sections.

In the case of elastic Ps scattering we see resonance structures near the Ps ionization threshold for all target molecules. At velocities above the ionization threshold we see good agreement between Ps scattering cross sections and electron scattering cross sections for the targets with smaller dipole moments, CO and HCl. However, we do not see such a similarity for LiF, which suggests that the similarity between electron and Ps scattering does not extend to highly polar targets.

At low velocities there is no direct similarity between electron and Ps scattering by the presently studied target molecules. This is not necessarily surprising due to the very different

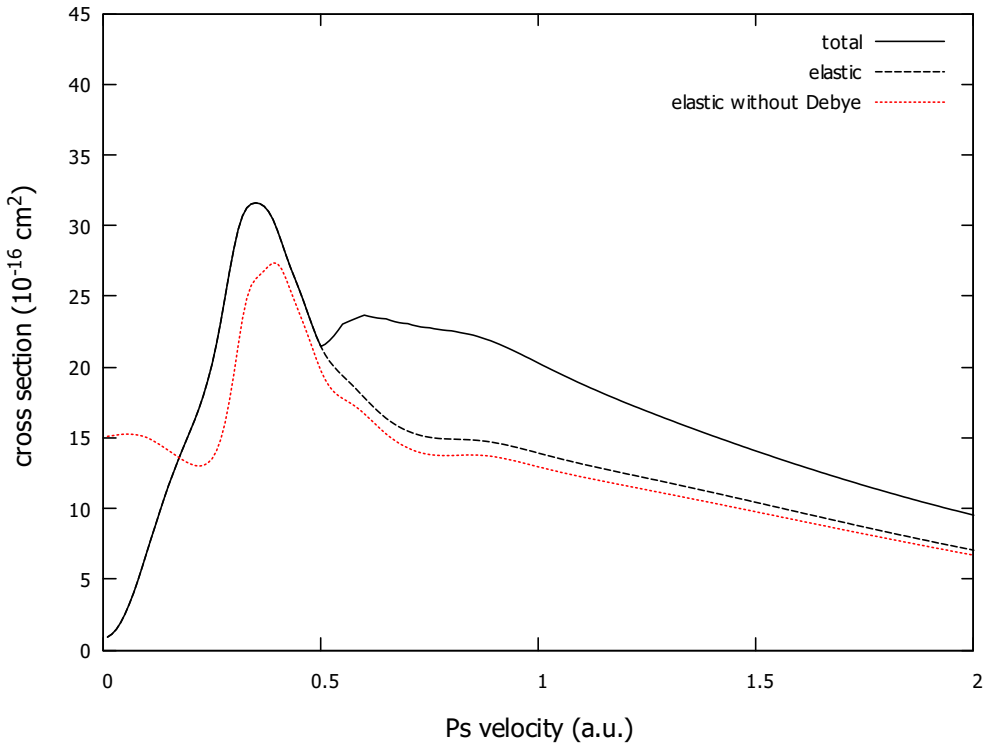

FIG. 13. Elastic Ps-LiF (dashed line) and total Ps-LiF (solid line)cross-sections. The dotted line is the elastic Ps-LiF cross section without inclusion of the Debye interaction.

long-range behavior of the scattering potentials in the two cases. In the case of Ps scattering the dipole moment has a much weaker effect than in the case of electron scattering. As for the non-polar molecules we have studied before, we see resonance structures in Ps scattering for all of the molecules that we have studied. For CO and LiF these resonance structures occur near or just below the Ps ionization threshold while for HCl they appear closer to zero velocity.

In the future we plan on extending the present model to study Ps-H_2O scattering for which experimental data is available. Also, we hope that the present results provide a basis to study Ps scattering by a crystal LiF surface, which has also been studied experimentally [67].

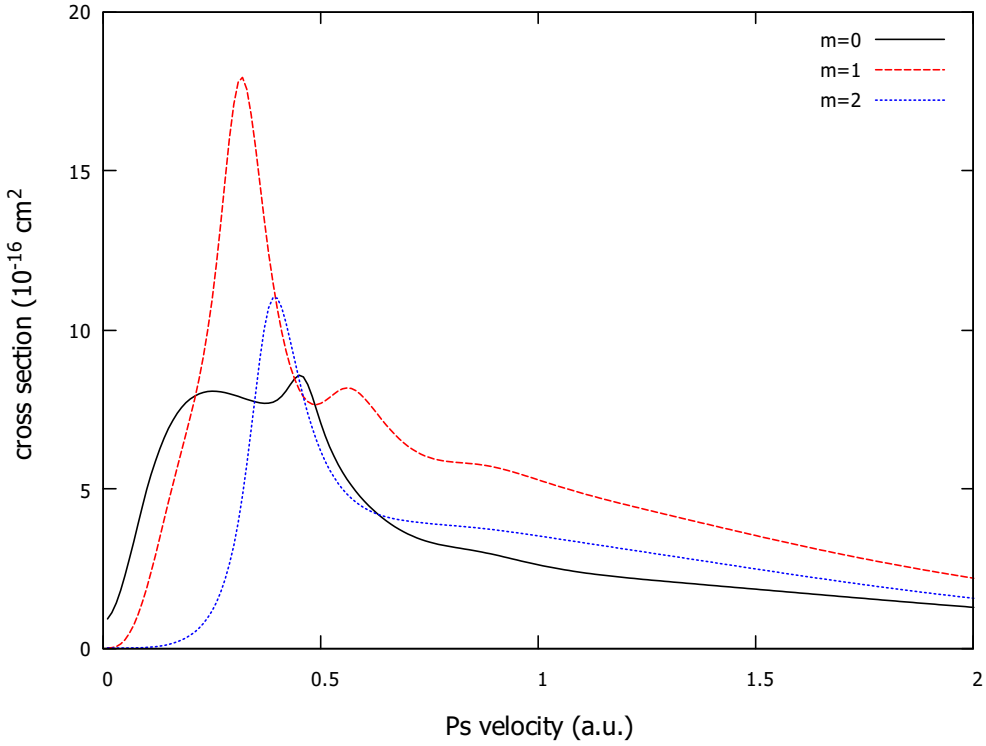

FIG. 14. Partial Ps-LiF elastic scattering cross sections. Solid line: $m = 0$, red ashed line: $m = 1$ and blue dotted line: $m = 2$, where m is the quantum number describing the projection of the Ps center of mass angular momentum on the internuclear axis.

ACKNOWLEDGMENTS

This work has been partly supported by the National Science Foundation, Grant Nos. PHY-1803744 and PHY-2011262.

[1] S. J. Brawley, S. Armitage, J. Beale, D. E. Leslie, A. I. Williams, and G. Laricchia, Science **330**, 789 (2010).

[2] M. Shipman, S. J. Brawley, L. Sarkadi, and G. Laricchia, Phys. Rev. A **95**, 032704 (2017).

[3] S. J. Brawley, A. I. Williams, M. Shipman and G. Laricchia, Phys. Rev. Lett. **105**, 263401 (2010).

[4] B. I. Schneider, Phys. Rev. A **24**, 1 (1981).

[5] Y. Itikawa, J. Phys. Chem. Ref. Data **31**, 749 (2002).

[6] W. Sun, M. A. Morrison, W. A. Isaacs, W. K. Trail, D. T. Alle, R. J. Gulley, M. J. Brennan, and S. J. Buckman, Phys. Rev. A **52**, 1229 (1995).

[7] R. S. Wilde and I. I. Fabrikant, Phys. Rev. A **97**, 052708 (2018).

[8] R. S. Wilde, H. B. Ambalampitiya and I. I. Fabrikant, Phys. Rev. A **104**, 012810 (2021).

[9] I. I. Fabrikant and G. F. Gribakin, Phys. Rev. Lett. **112**, 243201 (2014).

[10] I. I. Fabrikant and G. F. Gribakin, Phys. Rev. A **90**, 052717 (2014).

[11] R. S. Wilde and I. I. Fabrikant, Phys. Rev. A **98**, 042703 (2018).

[12] W. R. Garrett, Phys. Rev. A **4**, 2229 (1971).

[13] I. I. Fabrikant, J. Phys. B: At. Mol. Opt. Phys. **49**, 22205 (2016).

[14] J. Beale, S. Armitage and G. Laricchia, J. Phys. B: At. Mol. Opt. Phys. **39**, 1337 (2006)

[15] S. J. Brawley, A. I. Williams, M. Shipman, G. Laricchia, J. Phys.: Conf. Series **388**, 012018 (2012)

[16] M. T. McAlinden, F. G. R. S. MacDonald, and H. R. J. Walters, Can. J. Phys. **74**, 434 (1996).

[17] J. E. Blackwood, C. P. Campbell, M. T. McAlinden and H. R. J. Walters, Phys. Rev. A **60**, 4454 (1999).

[18] J. E. Blackwood, M. T. McAlinden, and H. R. J. Walters, J. Phys. B **35**, 2661 (2002).

[19] G. F. Gribakin, A. R. Swann, R. S. Wilde, and I. I. Fabrikant, J. Phys. B **49**, 064004 (2016).

[20] D. G. Green, A. R. Swann, and G. F. Gribakin, Phys. Rev. Lett. **120**, 183402 (2018).

[21] J. Mitroy and I. A. Ivanov, Phys. Rev. A **65**, 012509 (2001).

[22] J. Mitroy and M. W. J. Bromley, Phys. Rev. A **67**, 034502 (2003).

[23] A. R. Swann and G. F. Gribakin, Phys. Rev. A **97**, 012706 (2018).

[24] J.-Y. Zhang, M.-S. Wu, Y. Qian, X. Gao, Y.-J. Yang, K. Varga, Z.-C. Yan and U. Schwingenschlögl, Phys. Rev. A **100**, 032701 (2019).

[25] I. I. Fabrikant and R. S. Wilde, Phys. Rev. A **97**, 052707 (2018).

[26] R. S. Wilde and I. I. Fabrikant, J. Phys. B **53**, 185202 (2020).

[27] S. Hara, J. Phys. Soc. Japan **22**, 710 (1967).

[28] J. K. O'Connell and N. F. Lane, Phys. Rev. A **27**, 1893 (1983).

[29] Q. Sun, X. Zhang, S. Banerjee, P. Bao, M. Barbry, N. S. Blunt, N. A. Bogdanov, G. H. Booth, J. Chen, Z.-H. Cui, J. J. Eriksen, Y. Gao, S. Guo, J. Hermann, M. R. Hermes, K. Koh, P. Koval, S. Lehtola, Z. Li, J. Liu, N. Mardirossian, J. D. McClain, M. Motta, B. Mussard, H. Q. Pham, A. Pulkin, W. Purwanto, P. J. Robinson, E. Ronca, E. R. Sayfutyarova, M. Scheurer,

H. F. Schurkus, J. E. T. Smith, C. Sun, S.-N. Sun, S. Upadhyay, L. K. Wagner, X. Wang, A. White, J. Daniel Whitfield, M. J. Williamson, S. Wouters, J. Yang, J. M. Yu, T. Zhu, T. C. Berkelbach, S. Sharma, A. Yu. Sokolov, and G. K.-L. Chan, J. Chem. Phys. **153**, 024109 (2020).

[30] Q. Sun, T. C. Berkelbach, N. S. Blunt, G. H. Booth, S. Guo, Z. Li, J. Liu, J. McClain, S. Sharma, S. Wouters, and G. K.-L. Chan, WIREs Comput. Mol. Sci. **8**, e1340 (2018).

[31] Q. Sun, J. Comp. Chem. **36**, 1664 (2015).

[32] http://cccbdb.nist.gov/

[33] O. P. Andrade, O. A. V. Amaral, T. L. Fonseca, and M. A. Castro, Mol. Phys. **100**, 1975 (2002).

[34] M. A. Morrison, in *Electron-Molecule and Photon-Molecule Collisions*, eds. T. Rescigno, V. McKoy and B. Schneider (Plenum Press, New York 1979), p. 15.

[35] B. M. Smirnov, in *The Physics of Electronic and Atomic Collisions*, eds. J. S. Risley and R. Geballe (University of Washington Press, Seattle, 1976), p. 701.

[36] M. R. Flannery, in *Rydberg States of Atoms and Molecules*, eds. R. F. Stebbings and F. B. Dunning (Cambridge University Press, Cambridge 1983), p. 393.

[37] C. Starrett, M. T. McAlinden, and H. R. J. Walters, Phys. Rev. A **72**, 012508 (2005).

[38] Y. Itikawa, J. Phys. Chem. Ref. Data **44**, 1 (1983).

[39] Ch. K. Kwan, Y. F. Hsieh, W. E. Kauppila, S. J. Smith, T. S. Stein, M. N. Uddin, and M. S. Dababneh, Phys. Rev. A **27**, 1328 (1983).

[40] A. Hamada, O. Sueoka, J. Phys. B: At. Mol. Opt. Phys. 27, 5055 (1994).

[41] N. T. Padial, D. W. Norcross and L. A. Collins, Phys. Rev. A **27**, 141 (1983).

[42] M. Vinodkumar, C. G. Limbachiya, M. Y. Barot and N. J. Mason, Eur. Phys. J D **66**, 74 (2012).

[43] J. Arponen and E. Pajanne, Ann. Phys. **121**, 343 (1979).

[44] E. Boronski and R. M. Nieminen, Phys. Rev. B **34**, 3820 (1986).

[45] A. Jain, Phys. Rev. A **41**, 2437 (1990).

[46] F. A. Gianturco, T. Mukherjee, and P. Paioletti, Phys. Rev. A **56**, 3638 (1997).

[47] W. Kohn and L. J. Sham, Phys. Rev. **140**, A1133 (1965).

[48] M. Kimura, O. Sueoka, A. Hamada and Y. Itikawa, Adv. Chem. Phys. **111**, 537 (2000).

[49] T. Mukherjee and N. K. Sarkar, J. Phys. B: At. Mol. Opt. Phys. **41**, 125201 (2008).

[50] T. Mukherjee, Phys. Rev. A **96**, 042709 (2017).

[51] N. Sinha, S. Singh and B. Antony, J. Phys. B **51**, 015204 (2018).

[52] N. T. Padial and D. W. Norcross. Phys. Rev. A **29**, 1742 (1984).

[53] F. A. Gianturco, P. Paioletti, and J. A. Rodriguez-Ruiz, Z. Phys. D **36**, 51 (1996).

[54] I. Tamm, in *Selected Papers*, edited by B. Bolotovskii, V. Frenkel, and R. Peierls (Springer, Berlin Heidelberg, 1991), p. 157.

[55] S. M. Dancoff, Phys. Rev. **78**, 382 (1950).

[56] M. Baldo and R. Pucci, Nuovo Cimento B **23**, 202 (1974).

[57] R. P. McEachran, D. L. Morgan, A. G. Ryman and A. D. Stauffer, J. Phys. B: At. Mol. Phys. **10**, 663 (1977).

[58] L. Chiari, A. Zecca, S. Girardi, E. Trainotti, G. Garcia, F. Blanco, R. P. McEachran, and M. J. Brunger, J. Phys. B: At. Mol. Opt. Phys. **45**, 215206 (2012).

[59] L. Chiari, A. Zecca, E. Trainotti, G. Garcia, F. Blanco, M. H. F. Bettega, S. d'A. Sanchez, M. T. do N. Varella, M. A. P. Lima, and M. J. Brunger, Phys. Rev. A **88**, 022708 (2013).

[60] L. Chiari, E. Anderson, W. Tattersall, J. R. Machacek, P. Palihawadana, C. Makochekanwa, J. P. Sullivan, G. Garcia, F. Blanco, R. P. McEachran, M. J. Brunger, and S. J. Buckman, J. Chem. Phys. **138**, 074301 (2013).

[61] D. D. Reid and J. M. Wadehra, J. Phys. B: At. Mol. Opt. Phys. **29**, L127 (1996).

[62] W. Tattersall, L. Chiari, J. R. Machacek, E. Anderson, R. D. White, M. J. Brunger, S. J. Buckman, G. Garcia, F. Blanco, and J. P. Sullivan, J. Chem. Phys. **140**, 044320 (2014).

[63] D. Edwards, D. Stevens, Z. Cheong, V. Graves, J. D. Gorfinkiel, F. Blanco, G. Garcia, M. J. Brunger, R. D. White, and J. P. Sullivan, Phys. Rev. A **104**, 042807 (2021).

[64] A. Zecca, L Chiari, A. Sarkar and M. J. Brunger, New J. Phys. **13**, 115001 (2011).

[65] O. Sueoka and A. Hamada, J. Phys. Soc. Japan **62**, 2669 (1993).

[66] L. Vušković, S. K. Srivastava and S. Trajmar, J. Phys. B At. Mol. Phys. **11**, 1643 (1978).

[67] M. H. Weber, S. Tang, S. Berko, B. L. Brown, K. F. Canter, K. G. Lynn, A. P. Mills, Jr., L. O. Roellig, and A. J. Viescas, Phys. Rev. Lett. **61**, 2542 (1988).